# Active Suppression of Aeroelastic Instabilities on a Forward-Swept Wing

T. E. Noll*
*Air Force Wright Aeronautical Laboratories, Wright-Patterson AFB, Ohio*
F. E. Eastep†
*University of Dayton, Dayton, Ohio*
and
R. A. Calico‡
*Air Force Institute of Technology, Wright-Patterson AFB, Ohio*

**Analytical studies were conducted to investigate the potential of using feedback control systems for preventing multiple aeroelastic instabilities occurring simultaneously in close proximity on a forward-swept wing configuration. With the addition of wing mounted external stores, the classical bending/torsion flutter instability can be driven to lower airspeeds into the vicinity of aeroelastic instabilities such as divergence and body freedom flutter more commonly associated with a forward-swept wing. For these studies a typical forward-swept wing configuration, adversely mass balanced to create dynamic characteristics similar to those caused by adding external stores, was investigated. For various wing root boundary conditions, the study resulted in the preliminary design of a two-surface control law that provided large speed improvements and adequate gain margins. Phase margins, however, were predicted to be low but could be enhanced by trading speed improvement. Currently there are no requirements for such a system on a forward-swept wing aircraft nor are there plans to carry external stores in the future. However, the purpose of this study was to establish concept feasibility so that the technology can be considered for future application during a design as an alternative or option for preventing aeroelastic instabilities.**

## Introduction

THE forward-swept wing has been long recognized as able to provide some improved performance benefits over the aft-swept wing design of a flight vehicle, provided the weight needed to solve the potential aeroelastic problems (divergence) could be made minimal. Thirty to forty years ago, the procedure considered for preventing divergence on a conventional metal wing was to reduce the bending deformation by increasing the bending stiffness. To obtain sufficiently high divergence speeds at moderate forward sweep angles, the increase in weight resulting from the additional bending stiffness became prohibitive. As a result, interest in the forward-swept wing reached a minimum. In the mid 1970s Krone[1] completed a study in which laminated composite materials were used in such a manner that the divergence speed of a cantilever forward-swept wing was improved to a desired airspeed with a minimum weight penalty. Since composite materials have higher specific stiffness and strength characteristics than conventional metals and have directional properties, the orientation of the composites in a particular direction can change the deformation of the wing under aerodynamic loading. This study spurred additional and renewed interest in the development of forward swept wing technology. Subsequently, the application of advanced composite materials as applied to forward-swept wings was thoroughly evaluated through detailed analytical studies[2,3] and wind tunnel tests.[4-6]

In many of the forward-swept wing studies performed prior to 1980, motion of the entire aircraft as a rigid body was ignored. When aeroelastic analyses[7,8] and tests[9] were conducted with the rigid body airplane modes included, a dynamic instability involving the rigid body pitch mode and the wing first bending mode was predicted well below the divergence speed of the cantilever wing. For a clamped forward-swept wing, the bending mode frequency was found to drop with increasing airspeed until it became zero and diverged. For the forward-swept wing aircraft free in rigid body pitch, the short period mode frequency increased with airspeed and coalesced with the wing first bending frequency causing body freedom flutter. Even though the coupling of the aircraft pitch mode and the wing bending mode was new for forward swept wings, it had occurred in rare instances in the past on straight or slightly aft swept wings.[10,11] Although body freedom flutter has been calculated to be more critical than divergence of a cantilever wing for selected aircraft configurations, the aeroelastician should not generalize these findings. It is conceivable that cantilever wing divergence may, for peculiar aircraft configurations, be the most critical aeroelastic instability. Therefore, divergence of a cantilever wing should not be disregarded in the development of any new and promising aeroelastic control procedures.

A more recent technique considered for preventing divergence and body freedom flutter involved the use of an active feedback control system. The principles and procedures of applying these concepts are well-documented as a result of the significant amount of research performed in the 1970s to develop active flutter suppression technology and in the early 1980s to advance digital flight control and adaptive control principles. Initial studies[12] on a forward-swept wing investigated separately the control of both static divergence and bending/torsion flutter on a cantilever configuration. The active suppression of body freedom flutter[7,13] associated with the unclamped forward swept wing was also later shown to be feasible.

Future weapon requirements driven by inflationary costs have defined the necessity for a multimission fighter. To obtain the multirole capability, a fighter aircraft will carry

Received April 27, 1983; revision received July 28, 1983. This paper is declared a work of the U.S. Government and therefore is in the public domain.

*Aerospace Engineer, Structures & Dynamics Division, Flight Dynamics Laboratory. Associate Fellow AIAA.

†Professor and Director of Graduate Aerospace Engineering. Associate Fellow AIAA.

‡Professor, Aerospace Engineering Dept. Member AIAA.

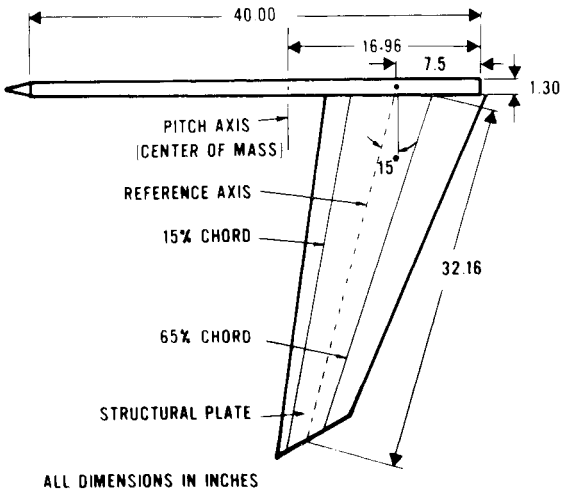


**Fig. 1 Planform of forward swept wing model.**

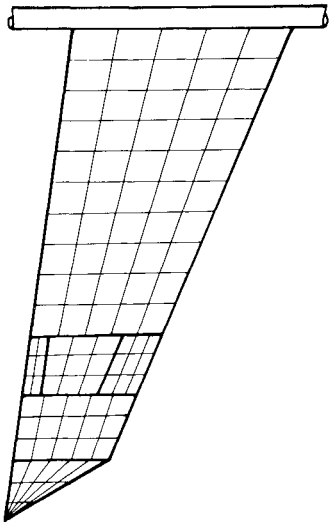

**Fig. 2 Aerodynamic panel representation of wing with leading and trailing edge control surfaces.**

external stores on the fuselage conformally and under the wings. It is expected that the forward-swept wing fighter will evolve in deployment and operational characteristics similar to those of the previous aft-swept wing fighters. Delivery to a target area of large amounts of external stores is a never-ending desire of an operational commander. However, the adverse mass and inertia distribution on the wings caused by the external stores have traditionally resulted in severe bending/torsion flutter problems. These stores may cause the higher frequency bending/torsion flutter mode of a forward-swept wing to be within the flight envelope of the vehicle and may result in a degradation of aircraft performance and survivability unless it is controlled simultaneously with the aeroelastic instability more commonly associated with the forward-swept wing.

The purpose of this research was to demonstrate by analyses the potential of active feedback control systems for simultaneously preventing both divergence and a high frequency bending/torsion flutter mode of a cantilever forward-swept wing, and for preventing the rigid body pitch/wing bending instability and flutter associated with the wing free in pitch. The goal was to increase the onset of the lowest instability speed 20% above the wing bending/torsion instability speed. This study does not represent an application to an existing aircraft, but to a configuration typical of what might be expected in the future. Also, there are currently no requirements for such an active control system on a forward swept wing aircraft or plans to consider the carriage of wing mounted external stores at this time. As such, various aspects of this study were simplified to provide a deeper insight and understanding of the mechanics and interactions involving flutter and the suppression techniques.

## Selected Model Configuration

Initial investigations were concentrated on obtaining a forward-swept wing configuration characterized as having a clamped divergence instability in close proximity to a classical bending/torison flutter mode, typical of what would occur if a critical external store configuration was carried. Figure 1 presents a schematic of the model selected for this study and shows the key details and dimensions and the relative sizes of the components.

To calculate the natural frequencies and mode shapes of the selected forward-swept wing configuration, a finite element[14] representation was developed. For all cantilever analyses, the fuselage bar was restrained in such a manner that no motion was permitted along the bar or wing root. When rigid body pitch was included in the analysis, the fuselage bar was permitted to pitch about the center of mass of the system. The elastic modes of interest for this study included the first two bending modes and the first torsion mode. Higher frequency modes were eliminated from the analysis when flutter analyses showed that they had essentially no effect on the instabilities of interest.

All aeroelastic instability analyses were conducted using classical flutter methods[15] and subsonic doublet lattice unsteady aerodynamics.[16] The aerodynamic paneling arrangement used in the flutter analysis is shown in Fig. 2. This paneling consisted of a fuselage with five interference panels and a wing with six aerodynamic panels subdivided into 104 boxes. Two of the outboard panels represent typical leading edge and trailing edge control surfaces that were investigated for use by the control system.

## Design Procedures

One classical technique for determining the aeroelastic stability of an aircraft with or without the presence of an active control system involves the use of root locus criteria. This section describes the basic development in transforming the equations of motion into a form suitable for the root locus procedures.

The aeroelastic equations of motion of a flexible aircraft in the airstream can be represented as

$$[M]\{\ddot{q}\} + [C]\{\dot{q}\} + [K]\{q\} = \{F\} \tag{1}$$

where $[M]$, $[C]$, and $[K]$ are the generalized mass, damping, and stiffness matrices obtained using a set of generalized coordinates $\{q\}$ and several natural vibration mode shapes, and $\{F\}$ represents the unsteady aerodynamic forces. For this study, the forces are obtained from the subsonic doublet lattice unsteady aerodynamic theory and are defined to be

$$\{F\} = -\tfrac{1}{2}\rho V^2 \bar{s}[Q(k)]\{q\} \tag{2}$$

where $\bar{s}$ represents a reference area.

The generalized aerodynamic force coefficient matrix $[Q]$ can be computed by

$$Q_{ij} = \int\int \frac{\Delta P_j}{\tfrac{1}{2}\rho V^2} \frac{h_i}{\bar{s}} \, dx \, dy \tag{3}$$

The coefficient $Q_{ij}$ represents the force in the $i$th mode due to pressure from the $j$th mode and is dependent on the reduced frequency $k$ where

$$k = \frac{b\omega}{V}$$

For zero initial conditions, the Laplace transform of Eq. (1) takes the form

$$\left[[M]s^2 + [C]s + [K] + \tfrac{1}{2}\rho V^2 \bar{s}[Q(s)]\right]\{q(s)\} = 0 \qquad (5)$$

The characteristic equation is obtained by setting the determinant of the coefficient matrix in Eq. (5) equal to zero. The roots of the resulting polynomial may be plotted in the complex plane as the velocity is varied.

Determining the roots requires that $[Q(s)]$ be specified. For the current analysis, we will assume that the elements of $[Q(s)]$ are given by

$$Q_{ij} = \left( \frac{N_0 + N_1 \frac{b}{V}s + N_2 \left(\frac{b}{V}\right)^2 s^2 + N_3 \left(\frac{b}{V}\right)^3 s^3}{1 + D_1 \frac{b}{V}s + D_2 \left(\frac{b}{V}\right)^2 s^2} \right)_{ij} \qquad (6)$$

which is a Pade polynomial[17] representation of the aerodynamic forces. The coefficients $N_i$ and $D_i$ were obtained using a least square fitting process over a reduced frequency range of interest. This fitting process was accomplished in two stages. In the first stage, unique numerator and denominator polynomials were obtained for each of the unsteady aerodynamic force coefficient elements. All the denominator polynomials were then averaged to define a common denominator for each element. During the second stage of the process, a least square fit was again accomplished; however, this time the denominator polynomials were constrained to the comon denominator previously obtained.

The aeroelastic equations of motion of a flexible aircraft with control surfaces present can be described as

$$[M]\{\ddot{q}\} + [C]\{\dot{q}\} + [K]\{q\} + \tfrac{1}{2}\rho V^2 \bar{s}[Q]\{q\} + [M_C]\{\ddot{q}_C\} + \tfrac{1}{2}\rho V^2 \bar{s}[Q_C]\{q\} = 0 \qquad (7)$$

where $[M_C]$ and $[Q_C]$ are the generalized masses and forces associated with each of the control surfaces. By obtaining Pade polynomials for the control surface aerodynamics and adding the feedback equations, the characteristic equation with feedback controls can be determined. The characteristic equation takes the form

$$[F_n]s^n + [F_{n-1}]s^{n-1} + \ldots + [F_1]s + [F_0] = 0 \qquad (8)$$

The roots of Eq. (8) can be found using conventional eigenvalue procedures.

Although it is realized that control surface displacements and rates are important in the design and effectiveness of a control law, the calculation of these quantities was not considered in this study. Also, sensor and actuator dynamics were neglected in these analyses. The control of divergence and the body freedom flutter instability was expected to be insensitive to actuator and sensor dynamics because of the low frequencies involved. However, it was anticipated that the control of the higher frequency wing bending/torsion flutter mode would be affected by the addition of these components. Previous active feedback control studies that have included the actuator and sensor characteristics in the analysis have shown that effective systems could be developed for significantly improving the flutter speeds of advanced vehicles.

## Results

The approach used in the development of the feedback compensation of the control system was to obtain gain loci for several sensor types and locations with different control surface inputs at a design airspeed (20% above the bending/torsion flutter speed). The data provided information to determine which sensor/control surface combination resulted in the best suppression capability for preventing the aeroelastic instabilities of each wing configuration. The various control system logics that provided model aeroelastic stability at the design airspeed were then analyzed at off-design conditions to assure stability over the entire velocity range of interest.

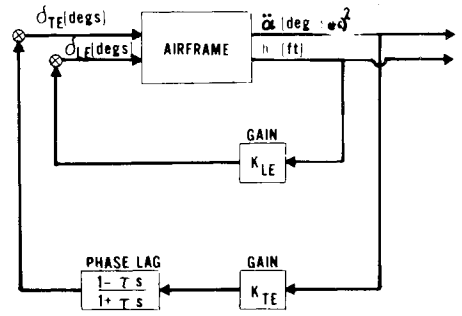


Fig. 3 Block diagram of two-surface control system, cantilever wing.

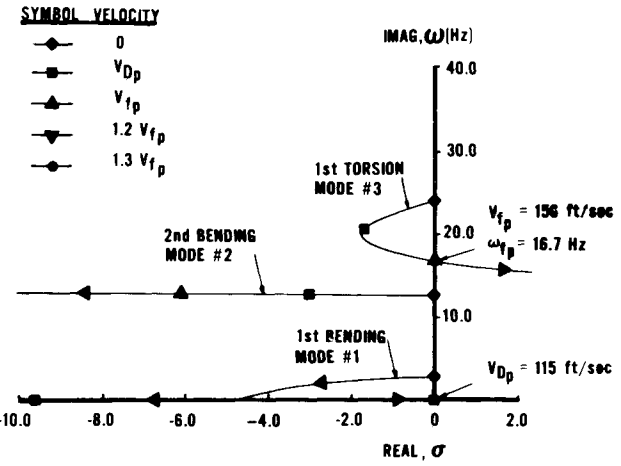


Fig. 4 Root locus plot for the cantilever wing, passive solution.

The results of these analyses indicated that a leading edge surface commanded by displacement feedback provided a reasonable control system design for preventing divergence of the cantilever wing or the body freedom flutter instability associated with the free model. The displacement sensor was positioned near the intersection of the wing second bending node line and the wing torsion node line. This location was best for feeding back the bending motion of the first elastic mode (critical mode for divergence or body freedom flutter) with minimum inputs from the other elastic modes. When the model was free, displacement at the wing sensor resulting from rigid model pitch was subtracted to obtain only a deflection due to the elastic modes. The sensor used for measuring rigid pitch was located at the model center of gravity on the fuselage bar (pitch axis).

Displacement feedback is a difficult state to measure directly. However, integration of an acceleration signal could provide the needed response. This technique of obtaining a displacement feedback results in significant changes in gain (20 db per frequency decade per integration) and phase characteristics (90 deg phase lag per integration). These changes would undoubtedly need to be accounted for in the final control law design if the double integration technique were used. Integration also offers the advantage of acting as a low pass filter and could be used to eliminate high frequency

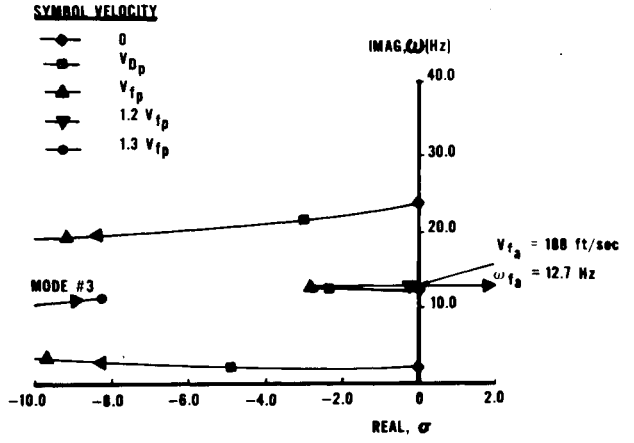


Fig. 5 Root locus for the cantilever wing, nominal two-surface control system ($K_{LE} = -5.2$, $K_{TE} = 0.0250$, $\phi_{TE} = 155$ deg, 17 Hz).

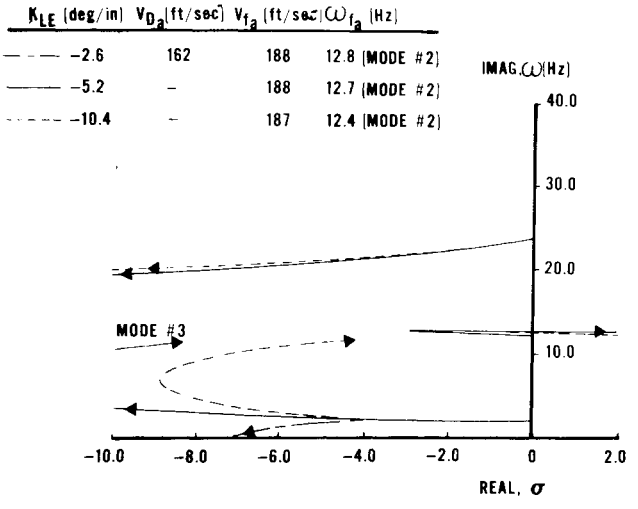


Fig. 6 Effect of leading edge gain variations, two-surface control system with $K_{TE}$ and $\phi_{TE}$ nominal, cantilever wing.

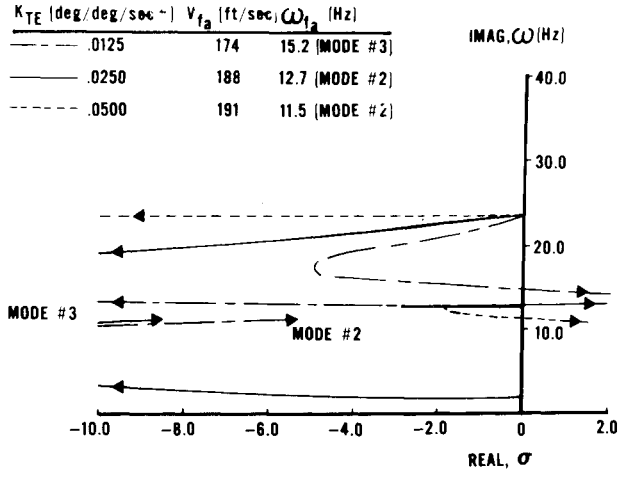


Fig. 7 Effect of trailing edge gain variations, two-surface control system with $K_{LE}$ and $\phi_{TE}$ nominal, cantilever wing.

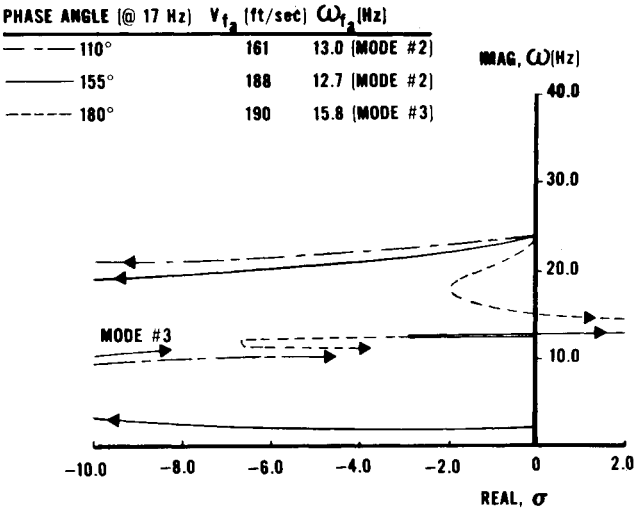


Fig. 8 Effect of trailing edge phase angle variations two-surface control system with $K_{LE}$ and $K_{TE}$ nominal, cantilever wing.

nonflutter responses (control system-induced structural instabilities).

These analyses also indicated that a trailing edge system commanded by angular acceleration of the wing tip perpendicular to the elastic axis provided an acceptable input for controlling the bending/torsion flutter mode. Based on mode shape data, the bending modes relative to the elastic axis had very little twist. Feeding back wing tip angular acceleration assured maximum input from the torsion mode (maximum twist at the tip) with minimum response from the bending modes.

For the limited analyses performed, the best overall capability consisted of the leading edge and trailing edge control surfaces positioned in the same streamwise location on the wing at about 75% span. Figure 3 presents a block diagram of the control system for the cantilever wing.

### Cantilever Wing

Figure 4 presents a velocity root locus plot for the cantilever wing with the active system off (passive solution). The passive divergence speed ($V_{D_p}$) was predicted to occur at 115 ft/s and the passive bending/torsion flutter speed ($V_{f_p}$) was predicted to occur at 156 ft/s at a passive flutter frequency ($\omega_{f_p}$) of 16.7 Hz. Classical flutter methods predicted a divergence speed of 119 ft/s and a wing bending/torison flutter speed of 155 ft/s at 16.9 Hz. Good correlation of the two techniques demonstrates the accuracy of the Pade polynomials.

For the augmented analyses, the design goal was to obtain a control law that would increase the flight speed of the model 20% above $V_{f_p}$ while obtaining gain margins of at least ±6 db and maximizing phase margins at $V_{f_p}$. A simple feedback control system was developed for suppressing the divergence and flutter tendencies of the cantilever wing configuration. Only gains and a phase lag network of the form $(1-\tau s/1+\tau s)$ were required for obtaining the goals established for this study. This type of phase lag network has been used extensively in operational analog simulations to verify control system phase margins. It is ideal for this use because large phase angles are possible with no gain changes. Such an element can easily be obtained in terms of operational amplifiers and potentiometers when hardware is required. Other techniques of including phase angle changes in the feedback system have also been used quite successfully in previous active flutter suppression analyses and tests.

During the design of the control law, a divergence system gain ($K_{LE}$) was first determined to provide the required speed improvement and to satisfy the gain margin requirements (±6 db) at $V_{f_p}$ on the leading edge system. It was found that with the flutter suppression system off, a $K_{LE}$ of −5.2 deg/in. was

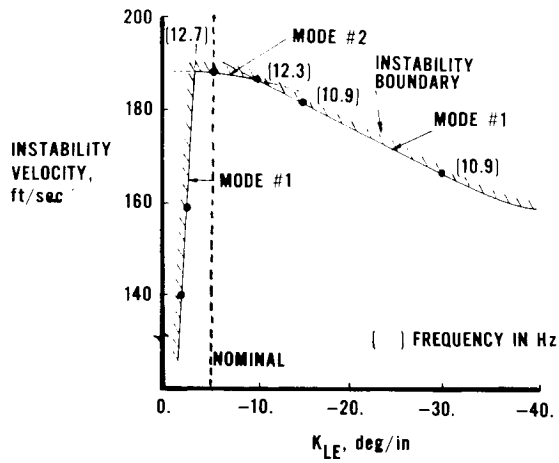


Fig. 9 Stability boundary with variable $K_{LE}$, cantilever wing.

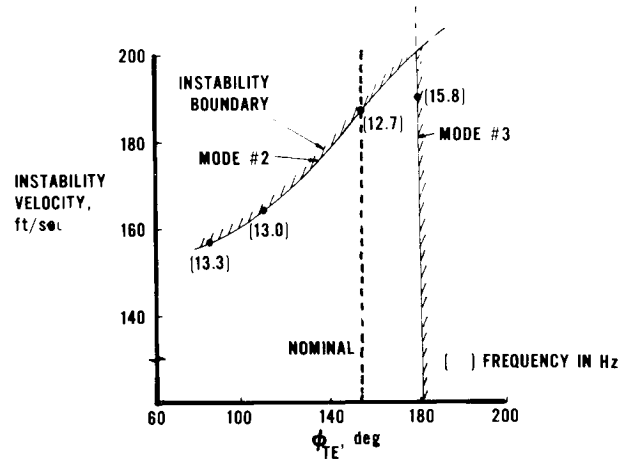


Fig. 11 Stability boundary with variable $\phi_{TE}$, cantilever wing.

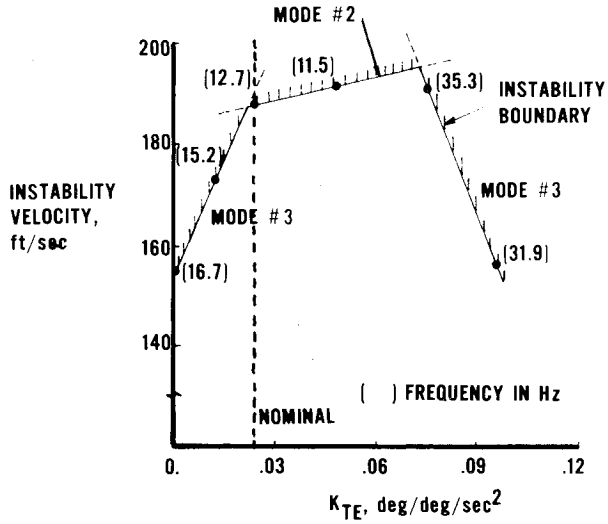


Fig. 10 Stability boundary with variable $K_{TE}$, cantilever wing.

required to achieve these goals. With this information known, the trailing edge gain and phase lag time constant were varied systematically until the flutter speed was increased to 1.2 $V_{f_p}$, and gain margins of ±6 db on the trailing edge system were obtained at $V_{f_p}$. At this time each of the feedback parameters was slightly perturbed to assure that minimums were obtained. The nominal two-surface control system was determined to have a leading edge surface gain of −5.2 deg/in., a trailing edge surface gain of 0.025 deg/deg/s$^2$ and a trailing edge phase lag network that provided 155 deg at reference frequency of 17 Hz. Figure 5 presents a root locus plot for the nominal two-surface control law. A 63% increase in the velocity above $V_{D_p}$ was achieved for this clamped configuration.

The analyses also indicated that the mode of instability can change as gains or the time constant in the phase lag network are varied from the nominal condition. Figure 6 shows that increasing $K_{LE}$ ($K_{TE}$ and $\phi_{TE}$ held constant at nominal) has a tendency to change a mode of instability that involved the second bending mode to an instability involving the first bending mode. Figures 7 and 8 present root locus plots for increasing $K_{\mathrm{TE}}$ (nominal $K_{LE}$ and $\phi_{TE}$) and $\phi_{TE}$ (nominal $K_{LE}$ and $K_{TE}$), respectively. Increasing $K_{TE}$ resulted in higher effective torsional stiffness which decoupled the flutter critical elastic modes. However, this also caused a control-induced instability in the second bending mode. As $K_{TE}$ was increased beyond 0.05 deg/deg/s$^2$ a more classical switch in the mode of intability was encountered. For this case, the mode changed from the second bending to a control induced torsion instability. As illustrated in Fig. 8, increasing $\phi_{TE}$ resulted in a change in the mode of instability from the second bending to the torsion mode.

Stability boundaries for the two-surface control law are provided in Fig. 9 through 11. The stability boundaries were determined with respect to each of the feedback parameters ($K_{LE}$, $K_{TE}$, and $\phi_{LE}$). The solid circles on the boundaries represent data taken from the root locus plots, and frequencies of the instability are shown in parentheses. The vertical dashed line represents the nominal control law. Once again, as one of the three parameters was varied, the other two were held constant at nominal values. Gain and phase margins can be easily determined from Fig. 9 through 11. This is accomplished by projecting a horizontal line through a reference velocity on the figure and reading the gains or phase angles at the instability boundaries that the line intersects. These gains and phase angles are then compared to the nominal control law to determine the margins. These margins are factors of safety that are established for a control system design. These are needed to account for the uncertainties, either neglected or unknown, that were encountered in an analysis.

As $K_{LE}$ was varied from 0 to −40 deg/in. (Fig. 9), the stability boundary changed from static divergence (Mode No. 1) at low $K_{LE}$, to a dynamic instability involving the second bending mode at moderate $K_{LE}$, and finally to a dynamic instability involving the first bending mode at high $K_{LE}$. The intersection of the stability boundaries to the left of the nominal law represented the classical switching of modes of instability. The intersection of the boundaries to the right of the nominal law represented a switching of the origin of the mode of instability and appeared to be a smooth transition from one mode to the other. The gain margins on $K_{LE}$ calculated at $V_{f_p}$ (reference velocity) are −6.19 db and 18.74 db. This means that the gain could be decreased 51% or increased 8.6 times nominal before neutral stability was obtained.

Figure 10 presents a trend of stability boundary with $K_{TE}$. The intersection of the boundaries to the left of the nominal control law represents a transition from Mode No. 3 to Mode No. 2, while the intersection of boundaries to the right represented a classical switching of Mode No. 2 back to Mode No. 3. The gain margins on $K_{TE}$ at $V_{f_p}$ were found to be negative infinity and 12.64 db. The gain margin of negative infinity on the trailing edge surface was a result of selecting $V_{f_p}$ as a reference speed ($K_{TE}=0$) to measure gain and phase margins.

The stability boundary resulting from a variation in $\phi_{TE}$ is shown in Fig. 11. For this analysis the intersection of

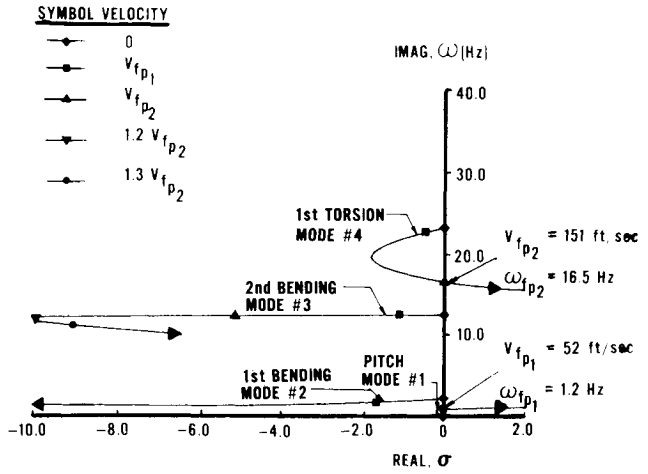


Fig. 12 Root locus plot for the model free in pitch, passive solution.

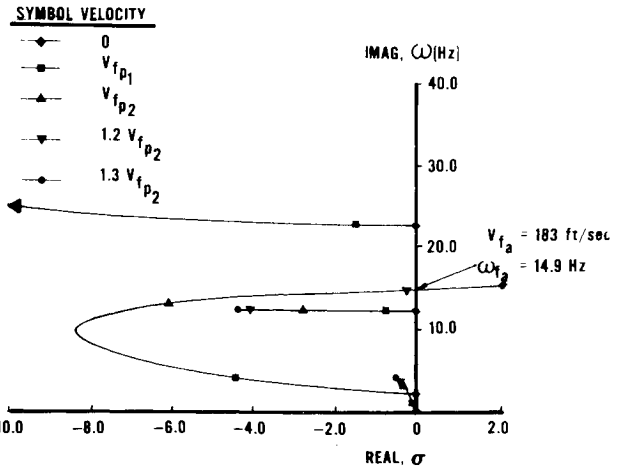


Fig. 13 Root locus for the model free in pitch, nominal two-surface control system ($K_{LE} = -122.0$, $K_{TE} = 0.026$, $\phi_{TE} = 173$ deg, 17 Hz).

boundaries was in the classical manner. The Mode No. 3 instability speed dropped very rapidly with phase angle changes slightly greater than 180 deg. The 155 deg phase lag at 17 Hz was the minimum phase angle at which a velocity improvement of 1.2 $V_{f_p}$ could be reached. The use of smaller phase angles in the control law resulted in lower speed increases but higher phase margins; higher phase angles resulted in a higher speed increase but lower phase margins. This trend continued up to about 182 deg, at which time further increases in phase angle caused low speed instabilities. The phase margins associated with the trailing edge loop were found to be $-70$ deg and 25 deg. Phase margins of at least $\pm 45$ deg could be obtained if the desired flight envelope expansion was limited to 53% (13% above $V_{f_p}$).

When the rigid body pitch degree of freedom was included in the analysis, it was determined, as expected, that static divergence was no longer a critical mode of instability for the forward swept wing. The coupling of the rigid pitch mode and the wing first bending mode of the forward swept wing caused a dynamic instability at speeds below the cantilever wing divergence speed. The next section will deal with the control and suppression of this low speed instability while simultaneously preventing the more classical higher frequency bending/torsion flutter mode.

### Model Free in Pitch

Figure 12 presents a velocity root locus plot for the model free in pitch with both feedback systems off (passive solution). The body freedom flutter instability was predicted to occur at 52 ft/s at 1.2 Hz, using aerodynamics approximated by Pade polynomials. The mode of instability for this case was the rigid pitch mode. This analysis also predicted the higher frequency bending/torsion instability to occur at 151 ft/s at 16.5 Hz. The classical flutter analysis techniques predicted a body freedom instability at 53 ft/s at 1.2 Hz. Bending/torsion flutter was determined to occur at 156 ft/s at 16.0 Hz. Correlation of the passive flutter data was quite good, giving an indication that the aerodynamics were again accurately represented by the Pade polynomials.

The control law for the model free in pitch was developed similar to the approach used for the cantilever wing. The block diagram for this configuration was similar to the schematic shown in Fig. 3 for the clamped wing with the exception of a sensor added in the leading edge system to provide rigid pitch motion. Wing tip angular acceleration was again fed back to the trailing edge control surface for suppressing the bending/torsion flutter mode. The feedback gains and the trailing edge phase lag network were of course different for this configuration.

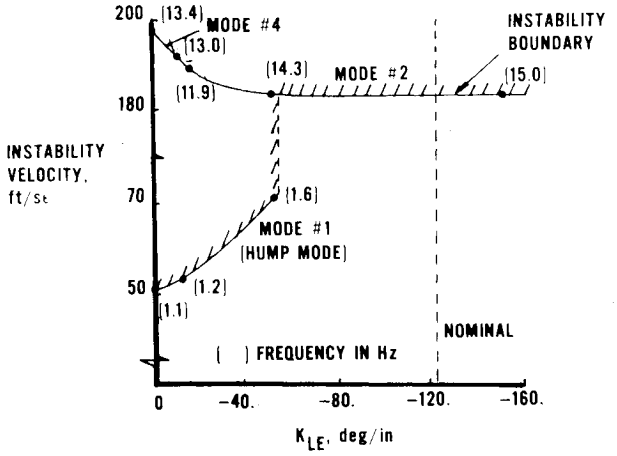


Fig. 14 Stability boundary with variable $K_{LE}$, model free in pitch.

To design the control law the leading edge gain ($K_{LE}$) was increased until the body freedom flutter speed exceeded 1.2 $V_{fp2}$ with gain margins of $\pm 6$ db at $V_{fp2}$. With $K_{LE}$ now known, the trailing edge system parameters were determined to obtain a total system instability speed of 1.2 $V_{fp2}$ with trailing edge gain margins of at least $\pm 6$ db at $V_{fp2}$ and maximum phase margins. The feedback parameters of the two-surface control law for the model free in pitch were found to have values of $-122$ deg/in. for $K_{LE}$, 0.026 deg/deg/s$^2$ for $K_{TE}$ and 173 deg at 17 Hz for $\phi_{TE}$. Figure 13 provides a velocity root locus of the wing with the two-surface control law operating. This control law increased the flight envelope of the configuration to 1.2 $V_{fp2}$ thus providing a 248% increase in the body freedom flutter speed.

The effects of varying the three feedback parameters separately from the nominal two-surface control law are presented in Figs. 14 to 16. Each figure presents a perturbation of one of the feedback parameters while the other two were held constant at nominal values. Results of these analyses are similar in terms of the potential instability switching mechanisms, as were seen for the cantilever wing. Three forms of mode switching were found for the model free in pitch. The first form of mode switching is demonstrated in Fig. 14. This figure shows the appearance of a low speed hump mode instability involving pitch (Mode No. 1); the hump mode became stable when the absolute value of $K_{LE}$ was greater than about 60 deg/in., causing a jump to a higher speed instability in the first elastic mode (Mode No. 2). The

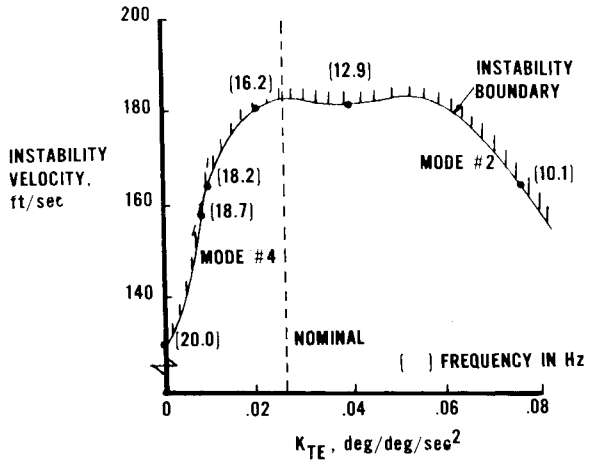


Fig. 15 Stability boundary with variable $K_{TE}$, model free in pitch.

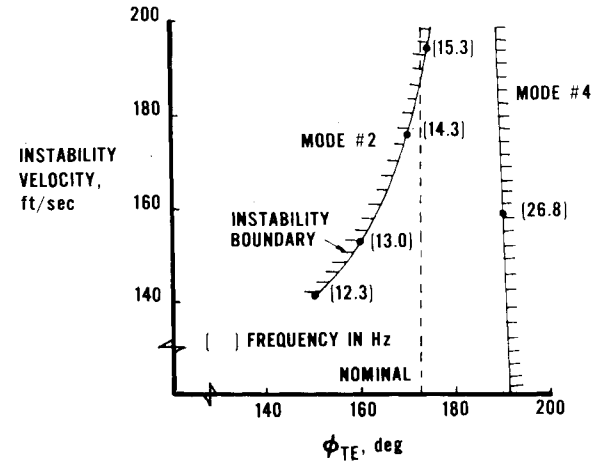


Fig. 16 Stability boundary with variable $\phi_{TE}$, model free in pitch.

second form involved a switching in the origin of the mode of instability. This mechanism, experienced when $K_{TE}$ was increased, is shown in Fig. 15. The frequency and modal characteristics of Mode No. 4 were gradually altered to a condition where the instability changed to the characteristics of Mode No. 2. The third type of instability mode switching was encountered when phase lag was varied. This mechanism involved the more classical abrupt change in frequency as shown in Fig. 16.

The gain and phase margins at $V_{fp_2}$ were obtained from Figs. 14 to 16. The gain margins on the leading edge system at $V_{fp_2}$ were found to be $-6.00$ db and positive infinity, and on the trailing edge system, $-12.74$ db and 11.96 db. The phase margins on the trailing edge system were calculated to be $-13.0$ deg and 17.0 deg.

## Summary

Control laws consisting of several sensors and two active surfaces were developed using root locus stability criteria to suppress the aeroelastic instabilities associated with a forward-swept wing. Both a cantilever wing and a model free in rigid pitch were analyzed separately. For this study, the reduced frequency dependent unsteady aerodynamic force coefficients predicted by the doublet lattice method were found to be adequately approximated by low order Pade polynomials. The analyses indicated that gain margins of $\pm 6$ db on all modes were not difficult to obtain for each wing configuration studied. However, phase margins were predicted to be low and could not be greatly improved without more complicated control logics or through a tradeoff with velocity improvement. It was also determined by the analysis that variations of the feedback parameters from the nominal conditions could cause changes in the mode of instability. These changes were identified as either classical mode switching (abrupt changes in frequency) or a transition from one mode to another (continuous frequency variation). Finally, the objectives of preventing two modes of instability simultaneously using a simple feedback control system were accomplished. For a cantilever wing, the static divergence instability speed was increased along with the wing bending/torsion flutter speed 20% above the latter. This resulted in a 63% improvement in the usable flight envelope. For the model free in pitch, analyses predicted that for a similar flight envelope expansion, the body freedom flutter speed could be increased 248% using an active system.

## References

[1] Krone, N., "Divergence Elimination with Advanced Composites," AIAA Paper 75-1009, Aircraft Systems and Technology Meeting, Los Angeles, Calif., Aug. 1975.

[2] Weisshaar, T.A., "The Influence of Aeroelasticity on Swept Composite Wings," AFWAL-TR-80-3137, Nov. 1980.

[3] Triplett, W.E., "Aeroelastic Tailoring of a Forward Swept Wing and Comparisons with Three Equivalent Aft Swept Wings," AIAA 21st SDM Conf., Seattle, Wash., May 1980.

[4] Sherrer, V.C., Hertz, T.J., and Shirk, M.H., "Wind Tunnel Demonstration of the Principle of Aeroelastic Tailoring Applied to Forward Swept Wings," AIAA Paper 80-0796, Seattle, Wash., May 1980.

[5] Wilkinson, K. and Rauch, F., "Predicted and Measured Divergence Speeds of an Advanced Composite Forward Swept Wing Model," AFWAL-TR-80-3039, July 1980.

[6] Ellis, J.W., Dobbs, S.K., and Miller, G.D., "Structural Design and Wind Tunnel Testing of a Forward Swept Fighter Wing," AFWAL-TR-80-3073, July 1980.

[7] Miller, G.D., Wykes, J.H., and Brosnan, M.J., "Rigid Body-Structural Mode Coupling on a Forward Swept Wing Aircraft," AIAA Paper 82-0683, New Orleans, La., May 1982.

[8] Weisshaar, T.A., "Divergence Suppression of Forward Swept Wings," Final Report, NASA Grant, NASI-15080-Task #16, Virginia Polytechnic Institute and State University, Sept. 1980.

[9] Weisshaar, T.A., Zeller, T.A., Hertz, T.J., and Shirk, M.H., "Flutter of Forward Swept Wings, Analysis and Test," Paper, 23rd AIAA SDM Conference, New Orleans, La., April 1982.

[10] Gaukroger, D.R., "Wind Tunnel Flutter Tests on Model Delta Wing under Fixed and Free-Root Conditions," British A.R.C., R&M 2826, 1955.

[11] Cunningham, H.J. and Lundstrom, R.R., "Description and Analysis of a Rocket-Vehicle Experiment on Flutter Involving Wing Deformation and Body Motions," NACA TN-3311, Jan. 1955.

[12] Griffin, K.E. and Eastep, F.E., "Active Control of Forward Swept Wings with Divergence and Flutter Aeroelastic Instabilities," AIAA Paper 81-0637, Atlanta Ga., April 1981.

[13] Chipman, R.R., Zislin, A.M., and Waters, C., "Active Control of Aeroelastic Divergence," Paper 82-0684, New Orleans, La., AIAA May 1982.

[14] The NASTRAN User's Manual, (Level 17.0), NASA SP-222 (04), National Aeronautics and Space Administration, Dec. 1979.

[15] "FASTOP-3: A Strength, Deflection and Flutter Optimization Program for Metallic and Composite Structures," AFFDL-TR-78-50, Vol. II, May 1978.

[16] Giesing, J.P., Kalman, T.P., and Rodden, W.P., "Subsonic Unsteady Aerodynamics for General Configurations," AFFDL-TR-75-5 Part I, Vols. I and II, Nov. 1971.

[17] Vepa, R., "On the Use of Pade Approximants to Represent Unsteady Aerodynamic Loads for Arbitrary Small Motions of Wings," AIAA Paper 76-17, Jan. 1976.